Journal of Physics: Conference Series **107** (2008) 012002 doi:10.1088/1742-6596/107/1/012002

Theoretical model for the detection of charged proteins with a silicon-on-insulator sensor

Stefan Birner, Christian Uhl, Michael Bayer and Peter Vogl

Walter Schottky Institute and Physics Department, Technical University of Munich, Am Coulombwall 3, 85748 Garching, Germany

E-mail: stefan.birner@nextnano.de

Abstract. For a bio-sensor device based on a silicon-on-insulator structure, we calculate the sensitivity to specific charge distributions in the electrolyte solution that arise from protein binding to the semiconductor surface. This surface is bio-functionalized with a lipid layer so that proteins can specifically bind to the headgroups of the lipids on the surface. We consider charged proteins such as the green fluorescent protein (GFP) and artificial proteins that consist of a variable number of aspartic acids. Specifically, we calculate self-consistently the spatial charge and electrostatic potential distributions for different ion concentrations in the electrolyte. We fully take into account the quantum mechanical charge density in the semiconductor. We determine the potential change at the binding sites as a function of protein charge and ionic strength. Comparison with experiment is generally very good. Furthermore, we demonstrate the superiority of the full Poisson-Boltzmann equation by comparing its results to the simplified Debye-Hückel approximation.

1. Introduction

The quickly progressing technology of low-dimensional semiconductor nanostructures requires and depends on reliable predictive theoretical methods for systematically improving, designing and understanding the electronic and optical properties of such structures. The situation becomes even more complicated if these nanostructures are combined with biomaterials to form bio-sensors [1]. These sensors are gaining importance due to their large potential in commercial applications, like pH, protein, virus or DNA sensors (bio-chips). Ion-selective field effect transistors (ISFETs) usually contain biomaterials in an electrolyte and consist of a two-dimensional electron (or hole) gas (2DEG) in the semiconductor region where a source-drain voltage is applied in the 2DEG plane. The measured source-drain current depends on the electron density in the 2DEG. The goal is to influence the electron density in the 2DEG in a reproducible manner through changes in the electrostatic potential which are caused by the charge distribution inside the electrolyte and in the vicinity of the interface between the semiconductor and the electrolyte, i.e. the electrolyte acts through this field effect as a gate. Several variations of this concept are possible, e.g. instead of having a 2DEG one could use a nanowire with quantum confinement in two directions, and thus enhance the sensitivity due to the increased surface-to-volume ratio, or one could use an optical device where the electrostatic potential in the electrolyte modifies transition energies in quantum wells, quantum wires or even quantum dots. Modeling of such devices [2] is essential not only for analyzing and interpreting

experimental results, but also for verifying theoretical concepts, and for the understanding of how to efficiently improve sensitivity.

In this article, we present realistic models of the electrolyte solution, its interaction with the semiconductor device surface, and of the semiconductor device itself. We discuss detailed simulations of protein sensors based on silicon in order to demonstrate the applicability of this approach. In section 2, we describe how we solve the Schrödinger equation and calculate the charge density in the semiconductor region. Our method that models the charge density in the electrolyte is outlined in section 3. Comments about the numerical treatment of the coupled system of semiconductor and electrolyte equations are given in section 4. Details of previously performed relevant experiments, and the theoretical model of the sensor are discussed in section 5. In section 6, we present results of self-consistent calculations of the spatial charge and electrostatic potential distributions for various protein charges and different ion concentrations in the electrolyte. Finally, the calculated surface potential is compared with experiments. The results indicate that the full Poisson-Boltzmann equation is able to reproduce experimental data whereas the widely used Debye-Hückel approximation faces severe limitations.

2. Modeling the semiconductor

The charge distribution within a general semiconductor device is given by

$$\rho(\mathbf{x}) = e\left[-n(\mathbf{x}) + p(\mathbf{x}) + N_{\mathrm{D}}^{+}(\mathbf{x}) - N_{\mathrm{A}}^{-}(\mathbf{x}) + \rho_{\mathrm{fix}}(\mathbf{x})\right], \tag{1}$$

where e is the positive elementary charge, n and p are the electron and hole densities, and N_{D}^{+} and N_{A}^{-} are the ionized donor and acceptor concentrations, respectively. If required, fixed interface or volume charge densities ρ_{fix} can be taken into account. The electron and hole densities can be calculated classically within the Thomas-Fermi approximation or quantum mechanically if quantum confinement effects are important. The p-type doped silicon sensor that is investigated in this work is operated in the inversion regime. Hence, only a quantum mechanical treatment of the conduction band electrons close to the X points in the Brillouin zone is necessary. The contributions to the density of all other bands like the conduction bands at the Γ and L points, and the heavy, light and split-off hole valence bands are negligible. In bulk silicon there are six equivalent conduction band valleys close to the X points in the Brillouin zone that are described by ellipsoidal effective mass tensors with one longitudinal and two transverse masses, m_{l} and m_{t}, respectively. As these ellipsoidal mass tensors are oriented differently with respect to each other, we have to treat these minima separately, i.e. we have to consider three different valleys where each one is two-fold degenerate. The quantum mechanical electron charge density for each of these three valleys is given by

$$n(\mathbf{x}) = g_{\mathrm{v}} g_{\mathrm{s}} \sum_{n} |\Psi_n(\mathbf{x})|^2 \, f\left(\frac{E_n - E_{\mathrm{F}}(\mathbf{x})}{k_{\mathrm{B}} T}\right), \tag{2}$$

where $g_{\mathrm{s}} = 2$ is the spin degeneracy and $g_{\mathrm{v}} = 2$ is the valley degeneracy. Ψ_n and E_n are the wavefunctions and eigenstates of the three-dimensional Schrödinger equation and depend on the orientation of each of the three ellipsoidal mass tensors, i.e. each valley requires the solution of the Schrödinger equation. The occupation of the eigenstates is governed by the Fermi-Dirac distribution function f taking into account the local quasi-Fermi level $E_{\mathrm{F}}(\mathbf{x})$. k_{B} is Boltzmann's constant and T is the temperature.

We use a standard approach to calculate the energy levels and wavefunctions, namely the single-band effective mass Schrödinger equation within the envelope function approximation. We discretize this equation with a finite differences method and assume a parabolic energy dispersion [3]. For a semiconductor structure that is grown along the z direction and that is homogeneous along the x and y directions, the envelope functions $\psi_n(z)$ and the energies E_n of

the n quantized electronic states are obtained as the solutions of the one-dimensional Schrödinger equation

$$\left[-\frac{\hbar^2}{2}\frac{\partial}{\partial z}\left(\frac{1}{m_\perp(z)}\frac{\partial}{\partial z}\right)+E_\mathrm{c}(z)-e\phi(z)\right]\psi_n(z)=E_n\psi_n(z), \tag{3}$$

where $m_\perp(z)$ is one of the three effective mass tensor components along the growth direction z, i.e. m_l or m_t for (001)-oriented silicon. $\hbar$ is Planck's constant divided by 2π and $E_\mathrm{c}(z)$ represents the conduction band edge profile of the relevant valley and takes into account band offsets at material interfaces. $\phi(z)$ is the electrostatic potential which is obtained from solving Poisson's equation (eq. (6)). It includes the external bias potential and the internal potential resulting from mobile charge carriers and ionized impurities. For a one-dimensional device that is homogeneous along the x and y directions, the quantum mechanical electron charge density is calculated for each valley as

$$n(z)=g_\mathrm{v}g_\mathrm{s}\sum_n|\psi_n(z)|^2\,\frac{m_{||}(z)k_\mathrm{B}T}{2\pi\hbar^2}\ln\left(1+\exp\left(\frac{E_\mathrm{F}(z)-E_n}{k_\mathrm{B}T}\right)\right), \tag{4}$$

where the sum over n is only over the lowest occupied subbands. $m_{||}(z)$ is the effective mass in the (x,y) plane. Obviously, this value depends on the conduction band valley, i.e. for unstrained (001)-oriented silicon layers the ground state electron level is associated with the longitudinal electron mass and thus $m_{||}$ is the transverse mass m_t. For the other valleys where the transverse mass is oriented along the growth direction z, the parallel mass is calculated as $m_{||}=\sqrt{m_\mathrm{l}m_\mathrm{t}}$ (density of states mass). Equation (4) leads to discontinuous charge densities at material interfaces if the value of $m_{||}$ differs between neighboring materials. In order to avoid this, we calculate for each subband n the parallel mass $m_{||}$ according to Ref. [4].

Taking into account the charge neutrality requirement, we first solve the Schrödinger-Poisson equation self-consistently in the whole device with the equilibrium requirement that the Fermi level in the silicon layer is assumed to be constant at $E_\mathrm{F}=0$ eV. In this case, we solve the Poisson equation with von Neumann boundary conditions and obtain the built-in electrostatic potential. The boundary values of the built-in potential plus optionally applied bias potentials at ohmic or Schottky contacts are then used as Dirichlet boundary conditions for the Poisson equation in nonequilibrium calculations.

3. Modeling the electrolyte

An electrolyte is an aqueous solution containing dissolved ions (e.g. Na^+, Cl^-) that result from the dissociation of salts. Electrolytes that are used as bio-sensors are usually buffer solutions and therefore resist changes in H_3O^+ and OH^- ion concentrations (and consequently the pH) upon addition of small amounts of acid or base, or upon dilution. The concentrations of the ions that are contained in the buffer depend on the pH and the $pK'_{a,T}$ value (dissociation constant) and can be calculated using the well-known Henderson-Hasselbalch equation (eq. (B.4)). In addition, the $pK'_{a,T}$ value depends on temperature and on ionic strength in a self-consistent way. For instance, when using a phosphate buffer, the concentrations of the buffer ions at a particular pH are governed by three different $pK'_{a,T}$ values and thus it is extremely difficult to derive the concentrations analytically. However, they can be calculated numerically in an iterative scheme [5]. In Appendix B, we describe the details of our buffer model where we allow the variables pH, $pK'_{a,T}$ and ionic strength to vary with spatial coordinates. Such an approach is necessary for analytes that produce local charge variations in the electrolyte, e.g. a charged molecule that binds to the semiconductor device surface. Furthermore, a local variation of pH is critical for the operation of EnFETs (enzyme field effect transistors) where the enzyme reaction depends on the pH value.

The distribution of all ion charges in the electrolyte solution is governed by the nonlinear Poisson-Boltzmann equation which is composed of the Poisson equation (eq. (6)) and the equation that describes the charge density distribution in the electrolyte (eq. (5)). Conventionally, the Poisson-Boltzmann equation is linearized which leads to the Debye-Hückel approximation (Appendix A). However, as we will show in subsection 6.1 such a simplification is generally not applicable in real devices and only valid for special and very limited cases. The solution $\phi(\mathbf{x})$ of the Poisson-Boltzmann equation determines the charge density in the electrolyte at position $\mathbf{x}$

$$\rho(\mathbf{x}) = \sum_{i=1}^{N} z_i e c_{i,0} \exp\left(-\frac{z_i e\left(\phi\left(\mathbf{x}\right) - U_{\mathrm{G}}\right)}{k_{\mathrm{B}}T}\right), \tag{5}$$

where z_i is the ion valency, e is the positive elementary charge, $c_{i,0}$ is the bulk concentration of the ion species i and $k_{\mathrm{B}}T$ is the thermal energy of the system at temperature T. The bulk electrolyte potential $\phi(\infty)$ can be adjusted by varying the potential of the reference gate electrode U_{G} that is connected to the electrolyte (Dirichlet boundary condition). $\phi(\mathbf{x})$ is the electrostatic potential that is obtained by solving the nonlinear Poisson equation in the overall device self-consistently (eq. (6)). Interface reactions can be taken into account by the so-called site-binding model for amphoteric oxide surfaces [6, 7] where the adsorption and dissociation of H^+ and OH^- ions at the interface between the electrolyte and the oxide lead to interface charge densities which depend on both the electrostatic potential at the interface and the pH of the electrolyte. These interface charge densities simply have to be added to the charge density that enters the Poisson equation.

4. Modeling the coupled system of semiconductor and electrolyte

The electrostatics within the electrolyte and the semiconductor require the self-consistent solution of the Poisson and Schrödinger equations. Both equations are discretized on a nonuniform grid with a finite differences method. They are solved numerically by iterative methods that are described in more detail in Ref. [8]. We point out that we solve only one single Poisson equation which includes both the electrolyte as well as the semiconductor region. It reads

$$\nabla \cdot [\varepsilon_0 \varepsilon_{\mathrm{r}}(\mathbf{x}) \nabla \phi(\mathbf{x})] = -\rho(\mathbf{x}), \tag{6}$$

where ε_0 is the permittivity of vacuum and ε_{r} is the relative permittivity of either the electrolyte or any of the semiconductor or insulator materials. In regions where the electrolyte is present, the charge density $\rho(\mathbf{x})$ is described by eq. (5), and in regions where the semiconductor materials or the oxides are present, the typical semiconductor equation is used (eq. (1)) which may include a suitable sheet charge density at the interface between the semiconductor device and the electrolyte. We note that it is not necessary to solve the Schrödinger equation in regions where the quantum mechanical density is negligible or zero, e.g. in insulators. However, wavefunction penetration into the barrier materials (e.g. at Si/SiO_2 interfaces) is fully taken into account by including a small region of the barrier material into the Schrödinger equation. We have implemented eqs (1)–(6) and similar ones for the two- and three-dimensional Schrödinger equations into the software package next**nano**^{3} [9]. This enables us to model combined semiconductor-electrolyte systems in one [10], two and three dimensions for arbitrary geometries and material compositions.

5. Description of the geometry and composition of the protein sensor

5.1. Sensor structure

Here, we discuss a silicon-on-insulator (SOI) based thin-film resistor that we will model in detail in section 6. Indeed, such a device has been realized experimentally for chemical and biological

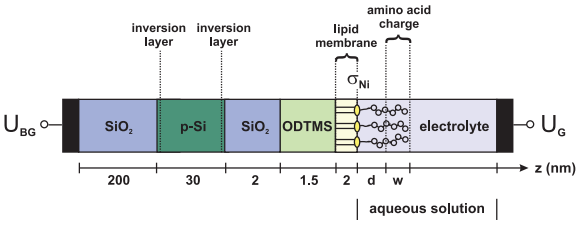

Figure 1. Schematic layout of the considered SOI structure. There is a negative interface charge density σ_{Ni} at the lipid/electrolyte interface. The amino acid charge is assumed to be distributed homogeneously over a width w. The electrolyte region includes the histidine-tagged amino acids as well as the neutral part of the tag of length d.

sensor applications [11, 12]. Peptides with a single charge can be detected and it is possible to distinguish single charge variations of the analytes even in physiological electrolyte solutions [13].

Figure 1 shows the layout of this bio-functionalized silicon-on-insulator device. It consists of a SiO_2-Si-SiO_2 structure. Specifically, we take a silicon dioxide buffer layer with a thickness of 200 nm and a conducting silicon layer of 30 nm which is homogeneously p-type doped with boron (doping density $p = 1 \cdot 10^{16}$ cm^{-3}). The silicon layer is covered by a native SiO_2 layer with a thickness of 2 nm. This oxide layer is passivated by an ODTMS (octadecyltrimethoxysilane) monolayer which is required for the bio-functionalization of the semiconductor device. We take a 1.5 nm thick oxide-like ODTMS layer and use a static dielectric constant of $\varepsilon_{\mathrm{r}} = 1.5$. Due to the passivation by ODTMS, we assume that no interface charges are present at the native oxide surface. The ODTMS layer is surface-functionalized with a lipid membrane that allows the specific binding of molecules. This lipid monolayer (2 nm) consists of DOGS-NTA (1,2-dioleoyl-*sn*-glycero-3-{[*N*(5-amino-1-carboxypentyl)iminodiacetic acid]succinyl}) incorporated into two matrix lipids (DMPC (1,2-dimyristoyl-*sn*-glycero-3-phosphocholine) and cholesterol). The lipid membrane is treated as an insulator using the same material parameters as for ODTMS. Thus, no charge carriers are assumed to be present within this layer. As the lipid layer is very dense, no electrolyte is considered within the lipid region.

For the ionic content of the electrolyte we consider a variable concentration of KCl (10, 50, 90 or 140 mM), and a fixed concentration of 1 mM of $NiCl_2$ and 1 mM of phosphate buffer saline (PBS) solution, respectively. The $NiCl_2$ dissociates into 1 mM of doubly charged cations and 2 mM of singly charged anions. For all calculations, the pH of the bulk electrolyte has been set to 7.5. The calculated concentrations of the PBS buffer ions are listed in table 1 for different salt concentrations. These values refer to the bulk electrolyte. In the vicinity of the semiconductor surface and in regions around charged analytes, however, the actual concentrations of the buffer ions vary locally. Our buffer model automatically takes this into account because the spatial variations of pH, ionic strength and $\mathrm{p}K'_{\mathrm{a},T}$ are determined self-consistently (see Appendix B for more details). The ionic strengths of the electrolyte solutions considered in this work, are largely dominated by the respective concentrations of singly charged anions and cations from KCl as can be seen in table 1. In these particular cases, i.e. small concentrations of PBS with respect to KCl, the Debye screening length is fully dominated by the KCl concentration.

The functionalized surface exposes NTA headgroups that carry two negative charges to the electrolyte solution. They have the ability to form a chelate complex with nickel ions if the latter are present in the solution. Upon loading with nickel, the charge of the headgroup changes by $+1e$ [14] and is then considered to be $-1e$. This results in a negative sheet charge density σ_{Ni} at the lipid/electrolyte interface. The surface density of the DOGS-NTA lipids is considered to be 5 % ($f_{\mathrm{NTA}} = 0.05$). The approximated headgroup area, i.e. the average area per functional DOGS-NTA is assumed to be $A_{\mathrm{NTA}} = 0.65$ nm^2. Consequently, the density of the headgroups is $s_{\mathrm{NTA}} = f_{\mathrm{NTA}}/A_{\mathrm{NTA}} = 7.7 \cdot 10^{12}$ cm^{-2}, so that the resulting charge density σ_{Ni} is given by $\sigma_{\mathrm{Ni}} = -e s_{\mathrm{NTA}}$, where we have assumed that each headgroup carries one negative charge upon exposure to Ni.

Table 1. Concentrations of ions in units of mM for several configurations of the electrolyte (1 mM PBS, 0 or 1 mM $NiCl_2$, pH = 7.5, $T = 25°C$). The ionic strength I and the Debye screening length κ^{-1} are also indicated.

Ion	0 mM KCl	10 mM KCl	50 mM KCl	90 mM KCl	140 mM KCl
$[H_2PO_4^-]$	0.303	0.256	0.214	0.192	0.176
$[HPO_4^{2-}]$	0.697	0.740	0.786	0.808	0.824
$[PO_4^{3-}]$	$0.135 \cdot 10^{-4}$	$0.206 \cdot 10^{-4}$	$0.335 \cdot 10^{-4}$	$0.430 \cdot 10^{-4}$	$0.524 \cdot 10^{-4}$
$[Na^+]$	1.697	1.740	1.786	1.808	1.824
$[K^+]$	0	10	50	90	140
$[Cl^-]$	0	10	50	90	140
$[Ni^{2+}]$	0	1	1	1	1
$[Cl^-]$	0	2	2	2	2
$[H^+]$	$0.316 \cdot 10^{-4}$	$0.316 \cdot 10^{-4}$	$0.316 \cdot 10^{-4}$	$0.316 \cdot 10^{-4}$	$0.316 \cdot 10^{-4}$
$[OH^-]$	$0.316 \cdot 10^{-3}$	$0.316 \cdot 10^{-3}$	$0.316 \cdot 10^{-3}$	$0.316 \cdot 10^{-3}$	$0.316 \cdot 10^{-3}$
I (mM)	2.393	15.481	55.573	95.616	145.648
κ (nm^{-1})	0.159	0.405	0.768	1.007	1.243
κ^{-1} (nm)	6.277	2.468	1.302	0.993	0.805

The charge carrier concentration of the conducting silicon layer is controlled by applying a backgate voltage U_{BG} which allows for switching between the accumulation (negative U_{BG}) and the inversion regime (positive U_{BG}) and particularly for tuning the sensitivity of the device. In all calculations that are mentioned in this work, the sensor is operated in inversion at $U_{BG} = 25$ V to allow for comparison with experiment. The experiment has shown that this is a compromise between the highest possible sensor signal and a low noise level. With this configuration, the p-doped silicon channel is inverted and becomes n-type. One can adjust the potential in the electrolyte by varying the voltage U_G of the reference electrode in the solution, mainly to vary the electron density of the right inversion layer with respect to the left one (see Figs. 1 and 2). In order to get a reasonable magnitude for the charge density in the right channel close to the functionalized surface, we have set $U_G = 1.0$ V for all calculations. These assumptions allow for a realistic comparison with specific protein binding experiments [13].

5.2. Model of the protein charge distribution

We consider two types of proteins: Aspartic acids and the green fluorescent protein. If divalent nickel ions (Ni^{2+}) are bound to the NTA headgroups of the lipid membrane, this surface functionalization then allows the specific coupling of histidine-tagged (his-tag) proteins or peptides to the membrane [14]. This process can be reversed by adding EDTA (ethylenediaminetetraacetic acid) to the electrolyte. A his-tag is a short amino acid sequence including histidines. They can be fused to one end of a protein and can also bind transition metal cations. We study a protein charge distribution that is spatially separated from the lipid membrane due to a neutral tag of width d in between the charged protein and the lipids. For simplicity, the protein charge is assumed to be distributed homogeneously over a width w.

5.2.1. Aspartic acid We consider an artificial protein structure where amino acids are tagged to a histidine chain. This artificial peptide binds to an NTA headgroup of the lipid membrane. A part of this artificial protein remains uncharged since no amino acids get attached there. By

contrast, the rest of the histidine backbone is negatively charged since we consider aspartic acids that carry one negative charge each for the binding to the tag. It is possible to manufacture the hexahistidine-tagged (His6) peptides with different numbers of charged residues, i.e. one can engineer the number of aspartic acids (Asp) that bind to the tag. The charge of the aspartic acids have been varied between carrying a single charge (His6Asp1) and up to ten charges (His6Asp10). It is expected that for each charge, a different signal can be detected and that peptides with higher charges result in an increased sensor response. The width of the neutral part has been taken to be $d = 2.3$ nm or $d = 2.8$ nm, depending on the concentration of KCl. The length of the uncharged part of the peptide consists of the length of the complete NTA headgroup including the spacer of 12 carbon atoms plus the his-tag. The width of the charged part

$$w(n) = n \cdot b \tag{7}$$

has been assumed to depend linearly on the number n of aspartic acid units and on the length b of one aspartic acid residue [13]. Thus, the spatial extent of the charge density increases with the number of aspartic acids. Each additional aspartic acid therefore shifts the center of the charge distribution about $b/2$ farther away from the lipid membrane. Additionally, we perform calculations where we keep this width w constant. The integrated charge density in the protein region changes in magnitudes of $-es_{\mathrm{NTA}}$ by increasing the number n of the aspartic acid units. Furthermore, we assume that the amino acid charges tend to repel each other. It is plausible that the strength of this repulsion is influenced by the ionic strength of the electrolyte. For that reason we reduce the length b of one aspartic acid unit at large ion concentrations. The electrolyte region starts at the membrane surface and includes the regions of both the neutral part of the tag and the protein charge distribution so that the ions in the aqueous solution screen the protein charge (Fig. 1).

5.2.2. Green fluorescent protein As a second protein, we consider the binding of the so-called green fluorescent protein (GFP) to the lipid membrane. GFP is also histidine-tagged to the NTA headgroups of the membrane. The size of GFP is larger (length of 4–5 nm) compared to his-tagged aspartic acids. We assume a charge distribution of width $w = 3.0$ nm that is connected with a neutral tag of width $d = 2.3$ nm to the NTA headgroups. At pH = 7.5, GFP carries eight negative charges that we assume to be homogeneously distributed over the protein region w.

6. Results of the calculations

Since we have specified all about the sensor and the proteins in the electrolyte, we are now ready to calculate the electrostatic potential in the semiconductor/electrolyte system for several protein charge distributions. The quantum mechanical charge densities are calculated self-consistently by solving the Schrödinger equation in the silicon channel. The Schrödinger and Poisson equations are coupled via the electrostatic potential and the charge densities.

First, we estimate the change in surface potential ϕ_{s} when one loads the NTA lipids with Ni^{2+}. We assume a sheet charge density change of $\Delta\sigma = -2es_{\mathrm{NTA}} - \sigma_{\mathrm{Ni}}$. We have actually calculated that the surface potential increases for a 140 mM KCl solution by 13.5 mV which is in agreement with the measurements [13].

Figure 2 shows the calculated conduction band edge and the electron density in the silicon channel for a backgate voltage of $U_{\mathrm{BG}} = 25$ V. Indicated is also the position of the Fermi level E_{F} and the electrostatic potential. Specifying a value for the potential U_{G} of the reference electrode is equivalent to a Dirichlet boundary condition for the electrostatic potential of the Poisson-Boltzmann equation. An increase of U_{G} leads to higher electron densities in the right channel. Therefore, the variation of U_{G} and the backgate voltage U_{BG} allows one to increase

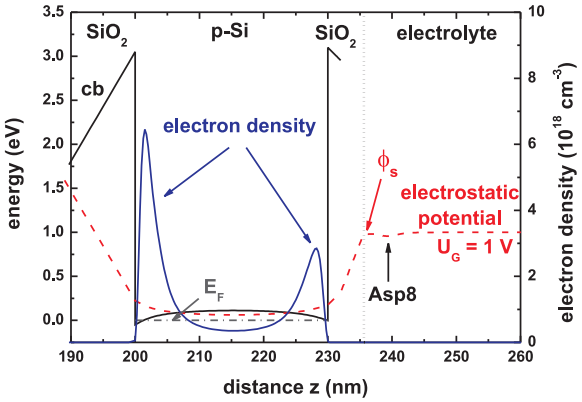

Figure 2. Calculated conduction band edge (black solid line) and electrostatic potential (dashed line) for the SOI structure at 50 mM KCl. The electron charge density (blue solid line) of the two inversion layers is shown. In the semiconductor, the Fermi level is set constant at $E_F = 0$ eV. Upon binding to the lipid membrane, the charge of the aspartic acid (Asp8) modifies the surface potential ϕ_s. The interface between the lipid membrane and the electrolyte is indicated by the vertical dotted line.

the sensitivity of the sensor by adjusting the ratio of the densities of the two channels. Our calculations yield channel densities of the order of a few 10^{12} cm^{-2}. They are modulated slightly by the actual configuration of the system in terms of ion concentrations and protein charges. Since a lower surface potential ϕ_s yields a lower electron density in the inverted silicon channel, the source-drain current is expected to decrease if negatively charged proteins bind to the functionalized sensor surface.

6.1. Influence of the protein charge on the sensitivity

In this subsection, we discuss results of the artificial protein that consists of several aspartic acids as described in subsection 5.2.1. For the 50 mM KCl solution, the neutral part of the histidine tag is assumed to have a width $d = 2.8$ nm and the respective protein charges are homogeneously distributed over a distance $w = nb$ where n is the number of aspartic acid units and $b = 0.3$ nm. For the 140 mM KCl solution, the respective values are $d = 2.3$ nm and $b = 0.1$ nm [13]. These parameters are reasonably close to the chemical structure of the histidine-tagged amino acids. Figure 3 shows the calculated potential distributions for a varying number of aspartic acids at 50 mM KCl. The magnitude of the negative protein charge density increases with the number of aspartic acids. This results in a lower electrostatic potential in the protein region. Also, the surface potential ϕ_s decreases with increasing protein charge. The region of the charged part of this protein is indicated schematically by the shaded triangle. We note that the electrolyte region starts at the lipid surface at 235.5 nm.

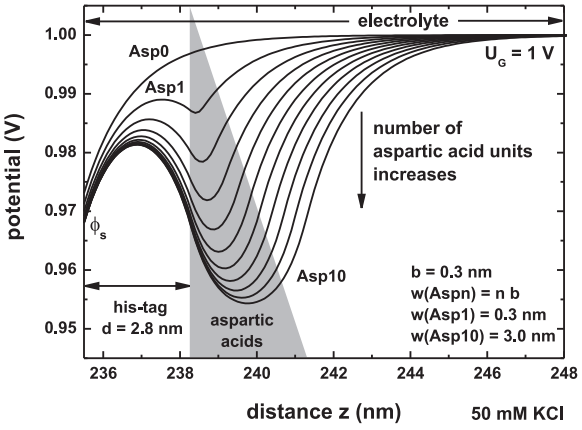

Figure 3. Calculated electrostatic potential distributions for varying protein charge at 50 mM KCl. Shown are the cases where no acids are bound and where the number of acids is $n = 1, 2, 3, ..., 10$. From top to bottom, the number of aspartic acids increases. The width w of the negative protein charge distribution is assumed to increase linearly with the number of aspartic acids. This width is indicated schematically by the shaded triangle.

In the following, we calculate the potential change at the interface between the lipid membrane

and the electrolyte as a function of the number of aspartic acids that are attached to each histidine tag for KCl concentrations of 50 mM and 140 mM. The reference level ϕ_s^{ref} for the scale of the surface potential change is set to the case for zero protein charge. The surface potential change $\Delta\phi_s$ is then defined as

$$\Delta\phi_s(n) = \phi_s^{ref} - \phi_s(n), \tag{8}$$

where n denotes the number of aspartic acid units. A positive potential change therefore implies that the reference level is higher compared to the situation with a nonzero number of aspartic acids. The results are shown in figure 4 and show excellent agreement with the experimental data of Ref. [13] where the surface potential was extracted from measurements of the sheet resistance of the silicon channel. Due to the lower ion concentrations in the case of 50 mM KCl, the protein charge density is less efficiently screened. Consequently, the surface potential change is larger compared to the case of 140 mM KCl. Therefore, the variation of the charge density in the silicon channel – and thus the sensitivity – is greater for a 50 mM KCl solution, as compared to 140 mM KCl.

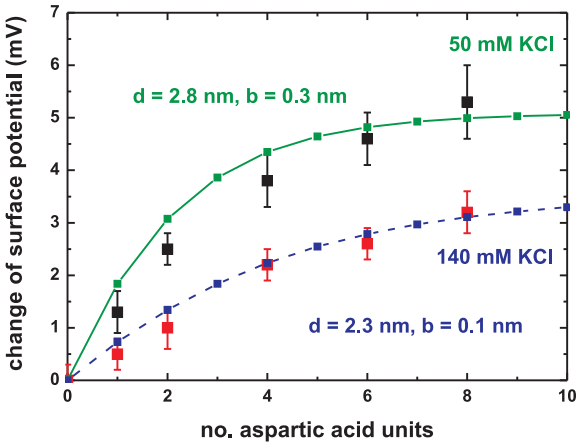

Figure 4. Calculated surface potential change at the lipid membrane as a function of the number of aspartic acids in the artificial protein. The solid line depicts the case of a KCl concentration of 50 mM whereas the dashed line represents the case of 140 mM KCl in the electrolyte solution. The experimental data points are from Ref. [13].

One important parameter of our model is the width d of the neutral part of the histidine tag. This distance between the lipid membrane and the beginning of the charge distribution of the aspartic acids influences the screening of the protein charges by ions in the solution. Hence, the impact of the amino acid charges decreases with increasing spacing of the lipid membrane, assuming the same protein charge distribution. This means that the influence on the semiconductor device can be enhanced by using a tag that allows small distances of the protein to the lipid membrane.

So far, we have considered homogeneous protein charge distributions where the width w has been varied as a function of the number of aspartic acid units n. In the following, we demonstrate that also a constant width w reproduces experimental data. Now, the number of aspartic acids solely determines the magnitude of the charge density but leaves the spatial extent of the peptide unchanged. For the 50 mM KCl solution, we use $d = 2.8$ nm and a constant width of $w = 1.5$ nm for all n. For the 140 mM KCl concentration, values of $d = 2.3$ nm and $w = 0.5$ nm are taken. The surface potential change as a function of the number of aspartic acids is illustrated in figure 5 for a protein charge of constant width w. Indicated are the results for both the Poisson-Boltzmann (PB) and the Debye-Hückel (DH) equation. The latter show a linear variation of the surface potential change with the number of aspartic acids. This is expected from the DH equation because a linear variation of the protein charge density leads to a linear variation of the surface potential change. In contrast, the results of the nonlinear PB equation resemble a logarithmic behavior and are in very good agreement with the experimental

data. This nonlinear dependence is attributed to screening effects in the electrolyte which cannot be reproduced correctly within the DH approximation (Appendix A). It is important to note that both assumptions, i.e. a constant width w and the linear variation of w with the number of aspartic acids n, reproduce experimental data, whereas the DH equation leads to unsatisfactory results. This emphasizes the importance of using the full PB equation rather than the linearized DH equation as it allows more insight into the screening of charges in electrolyte solutions. This is especially true if complex bio-functionalized surfaces are used where the binding of charged molecules occurs at about 5–10 nm from the surface, and where the prediction of the sensitivity limitations is desirable.

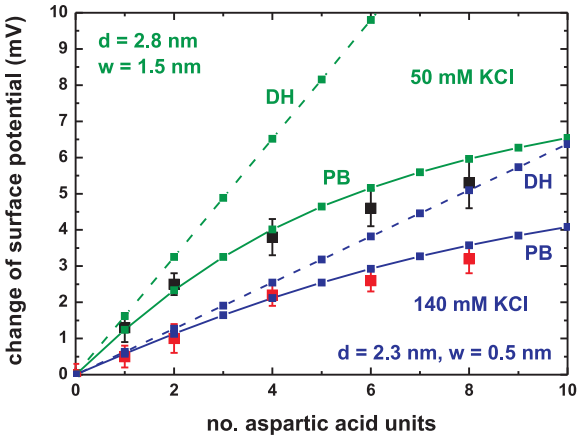

Figure 5. Calculated surface potential change as a function of the number of aspartic acids for two different salt concentrations (50 mM and 140 mM). Included are the results for the solution of the Poisson-Boltzmann (PB) equation (solid lines) and the Debye-Hückel (DH) equation (dashed lines). The latter show a linear dependence and deviate substantially from the PB results which are in good agreement with the experimental data.

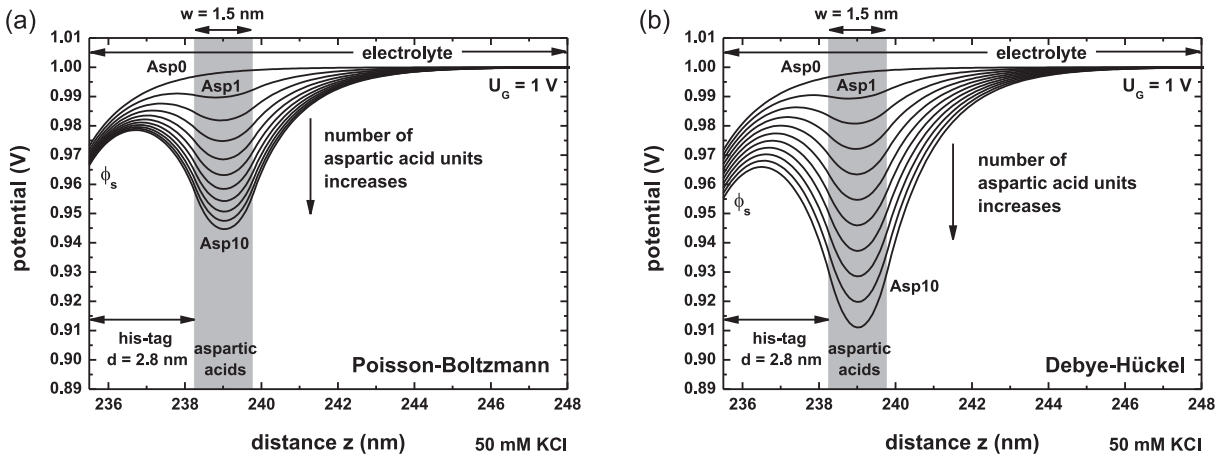

Figure 6. Calculated spatial potential distributions for (a) the full Poisson-Boltzmann equation and (b) the linearized Debye-Hückel equation for a negative protein charge distribution of constant width $w = 1.5$ nm. This width is indicated by the shaded region. Both figures include the solutions for different numbers of aspartic acids $n = 0, 1, ..., 10$.

The differences in the surface potential change that is either obtained within the full Poisson-Boltzmann theory or the simplified Debye-Hückel approximation can be further understood by investigating the spatial potential distributions in the electrolyte for different numbers of aspartic acids. This is shown in figure 6 where part (a) refers to the PB solutions and part (b) depicts the solutions of the DH approximation. Again, we have included the cases for integer numbers of aspartic acids n from 0 to 10. In both figures, the number of aspartic acids increases from the

top to the bottom. As one can see from figure 6(b), the potential differences at the membrane surface between adjacent potential solutions are constant. By contrast, the potential solutions in figure 6(a) do not show this behavior, in agreement with the experiment (see also Fig. 5).

6.2. Influence of the ionic strength on the sensitivity

In this subsection, we use the same sensor structure as in figure 1 but detect another protein. We consider the specific binding of the green fluorescent protein (GFP) to the lipid membrane and calculate the change of the surface potential as a function of the salt concentration (10, 50, 90 or 140 mM KCl) in the electrolyte. At pH = 7.5, GFP carries a net negative charge of $-8e$ as can be derived from the primary structure if one calculates the charge of the sidechains for the used buffer solution. Consequently, the integrated charge density of GFP is given by $\sigma_{\mathrm{GFP}} = -8e s_{\mathrm{NTA}}$. We assume for simplicity that this charge is distributed evenly over a distance of $w_{\mathrm{GFP}} = 3$ nm which is close to the length of the GFP (4–5 nm). Based on the previous section, the length of the neutral part of the tag has been taken to be $d = 2.3$ nm. Here, this length has been assumed to be the same for all KCl concentrations.

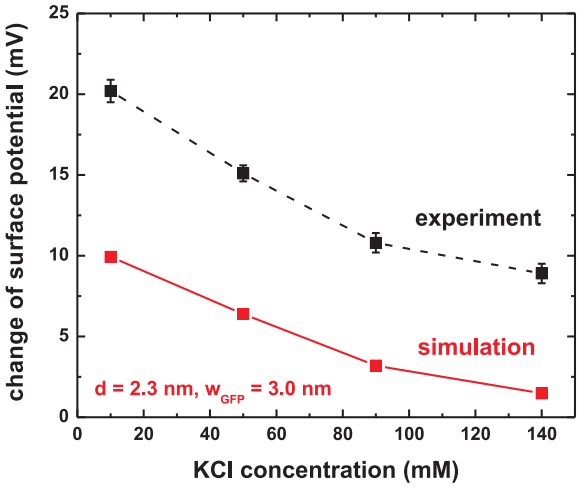

Figure 7. Calculated change of the surface potential as a function of the KCl concentration where we have assumed a charge distribution that resembles the green fluorescent protein. Included are experimental data of Ref. [13]. The lines are a guide to the eye.

We have calculated the change of the surface potential as a function of the KCl concentration in the electrolyte. The electrolyte has the same properties as for the aspartic acids (1 mM PBS, 1 mM $NiCl_2$). Figure 7 shows the results and compares them to the experimental data of Ref. [13]. The trend of the influence of the ionic strength on the sensitivity is well reproduced by our calculations. We note that the exact orientation of the GFP molecule at the surface is not known. A slight tilt angle can increase the measured sensor response due to the exponential dependence of the signal from the distance of the charges. The reduction of the spacing d or the width w_{GFP} of the charge distribution leads to larger surface potential changes. At higher ion concentrations, the Debye screening length of the electrolyte decreases, and thus the charges of the protein are more efficiently screened by the ions in the electrolyte. This leads to a reduced sensitivity which is approximately linear to the inverse of the Debye screening length. The Debye screening lengths of the different salt concentrations are listed in table 1.

7. Conclusions

We have presented calculations on the sensitivity of a silicon-on-insulator structure with respect to specific charge distributions in the electrolyte solution that may arise from protein binding to the semiconductor surface. Screening effects in the electrolyte have been taken into account using the Poisson-Boltzmann equation. The potential change at the bio-functionalized semiconductor

surface has been calculated for various protein charge distributions. Comparison with experiment is generally very good. We have demonstrated the superiority of the Poisson-Boltzmann equation by comparing its results to the simplified Debye-Hückel approximation. In agreement with experiment, we have found that the sensitivity of the structure is enhanced at low ion concentrations. We demonstrated that our numerical approach – the self-consistent solution of the Schrödinger and Poisson-Boltzmann equation – is well suited to model semiconductor based bio-sensors in a systematic manner, which is a requirement in order to both understand and optimize their sensitivity.

Acknowledgments
The authors acknowledge useful discussions with S. Luber, S. Q. Lud, M. G. Nikolaides and A. R. Bausch.

Appendix A. Debye-Hückel approximation

The full Poisson-Boltzmann equation is a nonlinear differential equation for the electrostatic potential. Very often, one is interested in reducing it to a simpler form which can be solved analytically. Within the Debye-Hückel approximation, the Poisson-Boltzmann equation is linearized by expanding the exponential of eq. (5) up to first order in ϕ so that the potential distribution in the electrolyte is governed by

$$\left(\nabla^2 - \kappa^2\right)\phi(\mathbf{x}) = 0, \tag{A.1}$$

where the Debye screening length is given by

$$\kappa^{-1} = \left(\sum_{i=1}^{N} \frac{\varepsilon_\mathrm{r}\varepsilon_0 k_\mathrm{B} T}{(z_i e)^2 c_{i,0}}\right)^{1/2}. \tag{A.2}$$

The Debye screening length is often used as a descriptive parameter of the system of investigation and is of the order of a few nanometers. However, the Debye-Hückel equation is only applicable for low electrostatic potentials where

$$e\phi(\mathbf{x}) \ll k_\mathrm{B} T. \tag{A.3}$$

Appendix B. Buffer solutions

To calculate the concentrations of the buffer ions, we briefly sketch the relevant equations that have been implemented into the self-consistent algorithm. See also Ref. [5] for more details on buffer solutions.

Appendix B.1. Ionic strength

The ionic strength of the electrolyte is defined as

$$I(\mathbf{x}) = \frac{1}{2}\sum_{i=1}^{N} c_i(\mathbf{x}) z_i^2 \tag{B.1}$$

where N is the number of all different ion species that are present in the electrolyte, c_i is the concentration and z_i is the valency of the ion species i. Because the concentrations of the ions in the vicinity of the semiconductor surface depend on the spatial coordinates, our algorithm allows for a spatially varying ionic strength. In physiological systems the ionic strength is of the order 150 mM.

Appendix B.2. Effect of temperature on buffers
The parameter $\mathrm{d}\mathrm{p}K_\mathrm{a}/\mathrm{d}T$ defines the change in $\mathrm{p}K_\mathrm{a}$ with temperature. This quantity depends on the buffer, and can be negative or positive or even close to zero.

$$\mathrm{p}K_{\mathrm{a},T} = \mathrm{p}K_\mathrm{a} + \mathrm{d}\mathrm{p}K_\mathrm{a}/\mathrm{d}T \cdot (T - 298.15\ \mathrm{K}) \tag{B.2}$$

Here, T is given in units of Kelvin and the 'thermodynamic' $\mathrm{p}K_\mathrm{a}$ value is defined for 25°C.

Appendix B.3. Debye-Hückel relationship
When using biological sensors, the pH is typically adjusted by titration and can be measured. Thus the pH of the bulk electrolyte is an input quantity for our simulations. Knowing the pH, one can calculate the concentrations of the buffer ions taking into account the temperature and the ionic strength of the solution. The $\mathrm{p}K'_{\mathrm{a},T}$ value determines the concentrations of the buffer ions but itself depends on the ionic strength $I(\mathbf{x})$ and on temperature T. As the ionic strength depends on the concentrations of the buffer ions, we have to solve this nonlinear equation self-consistently by an iterative scheme. The usually employed Debye-Hückel relationship reads

$$\mathrm{p}K'_{\mathrm{a},T} = \mathrm{p}K_{\mathrm{a},T} + (2z_a - 1)\left[\frac{A\sqrt{I}}{1+\sqrt{I}} - 0.1 \cdot I\right] \tag{B.3}$$

where $\mathrm{p}K'_{\mathrm{a},T}$ is called the 'modified' (or 'apparent' or 'working') $\mathrm{p}K_\mathrm{a}$ value, z_a is the charge on the conjugate acid species and the constant $A(T)$ depends on the temperature of the solution. The value of A is around 0.5 (at $T = 0°\mathrm{C} : A = 0.4918$, at $T = 100°\mathrm{C} : A = 0.6086$). $\mathrm{p}K'_{\mathrm{a},T}(\mathbf{x})$ is a function of position $\mathbf{x}$ because the ionic strength $I(\mathbf{x})$ is a function of position whereas $\mathrm{p}K_{\mathrm{a},T}$ only depends on the temperature.

Appendix B.4. Henderson-Hasselbalch equation
The Henderson-Hasselbalch equation relates the pH of the electrolyte to the $\mathrm{p}K'_{\mathrm{a},T}$ of the conjugate acid/base pair and the relative concentrations of acid and base.

$$\mathrm{pH} = \mathrm{p}K'_{\mathrm{a},T} + \log_{10}\frac{[\mathrm{base}]}{[\mathrm{acid}]} \tag{B.4}$$

Since all quantities of this equation depend on spatial coordinates, the local pH value is also a function of position. In the vicinity of the semiconductor surface, the local pH therefore differs from the pH of the bulk electrolyte. Most buffers involve only one chemical reaction, thus a single $\mathrm{p}K_\mathrm{a}$ value is sufficient. Some buffers are more complicated and involve three reactions, e.g. the phosphate buffer saline (PBS) solution, which is used in this work, requires three $\mathrm{p}K_{\mathrm{a}i}$ values ($i = 1, 2, 3$). As the concentrations of the ions also depend on the electrostatic potential through the Poisson-Boltzmann equation (eq. (6)) – which is influenced by the Schrödinger equation that determines the quantum mechanical charge density in the semiconductor device region – it is clear that only a numerical approach is feasible to solve this coupled system of equations self-consistently.

Appendix B.5. Phosphate buffer
Phosphate buffer saline (PBS) is made of orthophosphoric acid $\mathrm{H_3PO_4}$ and shows three dissociation reactions.

$$\mathrm{H_3PO_4} \overset{\mathrm{p}K'_{\mathrm{a}1,T}}{\rightleftharpoons} \mathrm{H_2PO_4}^- + \mathrm{H}^+ \overset{\mathrm{p}K'_{\mathrm{a}2,T}}{\rightleftharpoons} \mathrm{HPO_4}^{2-} + 2\mathrm{H}^+ \overset{\mathrm{p}K'_{\mathrm{a}3,T}}{\rightleftharpoons} \mathrm{PO_4}^{3-} + 3\mathrm{H}^+ \tag{B.5}$$

Table B1. Buffer parameters: Phosphate buffer saline (PBS).

Symbol	Value	Units
$\mathrm{p}K_{\mathrm{a}1}(25°\mathrm{C})$	2.15	
$\mathrm{p}K_{\mathrm{a}2}(25°\mathrm{C})$	7.21	
$\mathrm{p}K_{\mathrm{a}3}(25°\mathrm{C})$	12.33	
$\mathrm{d}\mathrm{p}K_{\mathrm{a}1}/\mathrm{d}T$	0.0044	K^{-1}
$\mathrm{d}\mathrm{p}K_{\mathrm{a}2}/\mathrm{d}T$	−0.0028	K^{-1}
$\mathrm{d}\mathrm{p}K_{\mathrm{a}3}/\mathrm{d}T$	−0.026	K^{-1}
z_{a1}	0	
z_{a2}	−1	
z_{a3}	−2	
$A(25°\mathrm{C})$	0.5114	

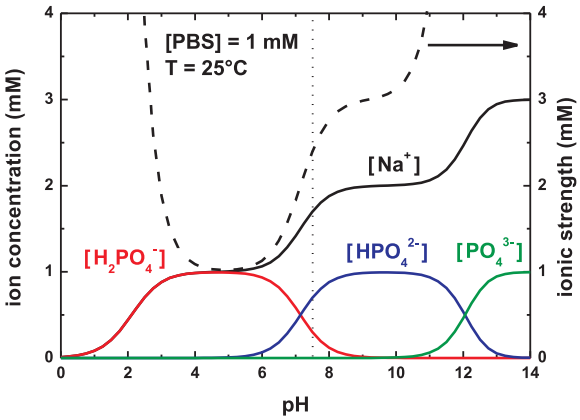

Figure B1. Calculated concentrations of the buffer ions (solid lines) of the phosphate buffer saline solution as a function of pH. At small and large pH values, the ionic strength (dashed line) strongly increases due to the increase in $[\mathrm{H_3O^+}]$ and $[\mathrm{OH^-}]$ concentrations, and their corresponding anions and cations. The influence of the valency on ionic strength (quadratic dependence, cf. eq. (B.1)) is very pronounced for $[\mathrm{HPO_4}^{2-}]$.

Using the Henderson-Hasselbalch equation (eq. (B.4)), the concentrations of the involved ions can be calculated by the following formulas:

$$[\mathrm{H_3PO_4}] = \frac{[\mathrm{PBS}]}{1 + 10^{\mathrm{pH}-\mathrm{p}K'_{\mathrm{a}1,T}} \cdot \left(1 + 10^{\mathrm{pH}-\mathrm{p}K'_{\mathrm{a}2,T}} \cdot \left(1 + 10^{\mathrm{pH}-\mathrm{p}K'_{\mathrm{a}3,T}}\right)\right)} \tag{B.6}$$

$$[\mathrm{H_2PO_4}^-] = [\mathrm{H_3PO_4}] \cdot 10^{\mathrm{pH}-\mathrm{p}K'_{\mathrm{a}1,T}} \tag{B.7}$$

$$[\mathrm{HPO_4}^{2-}] = [\mathrm{H_2PO_4}^-] \cdot 10^{\mathrm{pH}-\mathrm{p}K'_{\mathrm{a}2,T}} \tag{B.8}$$

$$[\mathrm{PO_4}^{3-}] = [\mathrm{HPO_4}^{2-}] \cdot 10^{\mathrm{pH}-\mathrm{p}K'_{\mathrm{a}3,T}} \tag{B.9}$$

$$[\mathrm{Na^+}] = -z_1 [\mathrm{H_2PO_4}^-] - z_2 [\mathrm{HPO_4}^{2-}] - z_3 [\mathrm{PO_4}^{3-}] \tag{B.10}$$

Here, $z_1 = -1$, $z_2 = -2$ and $z_3 = -3$ are the valencies of the respective ions $\mathrm{H_2PO_4}^-$, $\mathrm{HPO_4}^{2-}$ and $\mathrm{PO_4}^{3-}$. In our implementation, the concentration of the PBS buffer and the pH in the bulk electrolyte are fixed. However, the local value for the pH depends on the local concentration of $\mathrm{H_3O^+}$ ions. The concentrations of the buffer ions $[\mathrm{H_2PO_4}^-]$, $[\mathrm{HPO_4}^{2-}]$, $[\mathrm{PO_4}^{3-}]$ and $[\mathrm{Na^+}]$ are then calculated using the parameters listed in table B1. For a given local value of pH, eqs (B.1), (B.3) and (B.4) (i.e. eqs (B.6), (B.7), (B.8), (B.9) and (B.10)) have to be solved self-consistently in an iterative manner. Figure B1 shows the concentrations of the buffer ions and the ionic

strength as a function of pH for a 1 mM PBS buffer. The second column (0 mM KCl) of table 1 lists these values at pH = 7.5 (dotted line in Fig. B1).

Appendix C. Material parameters

Table C1 contains relevant material parameters that were used in the calculations.

Table C1. Material parameters.

Description	Symbol	Value	Units
longitudinal electron effective mass (Si)	m_l	0.916	m_0
transverse electron effective mass (Si)	m_t	0.190	m_0
static dielectric constant (Si)	ε_r	11.7	
static dielectric constant (SiO_2)	ε_r	3.8	
static dielectric constant (ODTMS)	ε_r	1.5	
static dielectric constant (electrolyte)	ε_r	80	

References

[1] Cui Y, Wei Q, Park H and Lieber C M 2001 "Nanowire Nanosensors for Highly Sensitive and Selective Detection of Biological and Chemical Species" *Science* **293** 1289–92
[2] Heitzinger C and Klimeck G 2007 "Computational aspects of the three-dimensional feature-scale simulation of silicon-nanowire field-effect sensors for DNA detection" *J. Comput. Electron.* **6** 387–90
[3] Tan I-H, Snider G L, Chang L D and Hu E L 1990 "A self-consistent solution of Schrödinger-Poisson equations using a nonuniform mesh" *J. Appl. Phys.* **68** 4071–6
[4] Davé D P and Taylor H F 1994 "Thomas-Kuhn sum rule for quantum mechanical systems with a spatially varying effective mass" *Phys. Lett. A* **184** 301–4
[5] Beynon R J and Easterby J S 1996 *Buffer Solutions: The basics* (New York: Oxford University Press)
[6] Bergveld P 1970 "Development of an ion-sensitive solid-state device for neurophysiological measurements" *IEEE Trans. Biomed. Eng.* **17** 70–1
[7] Healy T W and White L R 1978 "Ionizable surface group models of aqueous interfaces" *Adv. Colloid Interface Sci.* **9** 303–45
[8] Trellakis A, Zibold T, Andlauer T, Birner S, Smith R K, Morschl R and Vogl P 2006 "The 3D nanometer device project *nextnano*: Concepts, methods, results" *J. Comput. Electron.* **5** 285–9
[9] The next**nano**^{3} software can be obtained from `http://www.wsi.tum.de/nextnano3` and `http://www.nextnano.de`.
[10] Bayer M, Uhl C and Vogl P 2005 "Theoretical study of electrolyte gate AlGaN/GaN field effect transistors" *J. Appl. Phys.* **97** 033703
[11] Nikolaides M G, Rauschenbach S, Luber S, Buchholz K, Tornow M, Abstreiter G and Bausch A R 2003 "Silicon-on-Insulator Based Thin-Film Resistor for Chemical and Biological Sensor Applications" *ChemPhysChem* **4** 1104–6
[12] Nikolaides M G, Rauschenbach S and Bausch A R 2004 "Characterization of a silicon-on-insulator based thin film resistor in electrolyte solutions for sensor applications" *J. Appl. Phys.* **95** 3811–5
[13] Lud S Q, Nikolaides M G, Haase I, Fischer M and Bausch A R 2006 "Field Effect of Screened Charges: Electrical Detection of Peptides and Proteins by a Thin-Film Resistor" *ChemPhysChem* **7** 379–84
[14] Schmitt L, Dietrich C and Tampe R 1994 "Synthesis and Characterization of Chelator-Lipids for Reversible Immobilization of Engineered Proteins at Self-Assembled Lipid Interfaces" *J. Am. Chem. Soc.* **116** 8485–91